Beyond Traditional Poincaré Analysis: Second-Order Plots Reveal Respiratory Effects in Heart Rate Variability

Mikhail A Lebedev[1,2,3,*], Alexandra S Medvedeva[4], Ksenia P Solovieva[4,5], Nadezhda M Starodubtseva[5], Anna V Makarova[2], Daria F Kleeva[2,4,5]

[1]Faculty of Mechanics and Mathematics, Lomonosov Moscow State University, Moscow, Russia
[2]Research Center in the Field of Artificial Intelligence, Lomonosov Moscow State University, Moscow, Russia
[3]Sechenov Institute of Evolutionary Physiology and Biochemistry of the Russian Academy of Sciences, St. Petersburg, Russia
[4]MSU Institute for Artificial Intelligence, Moscow, Russia
[5]Institute for Information Transmission Problems of the Russian Academy of Sciences, Moscow, Russia
[*]Corresponding author: mikhail.a.lebedev@gmail.com

Abstract

Poincaré plots, which visualize heart rate variability (HRV) by plotting each RR interval (RR_i) against the subsequent one (RR_{i+1}), serve as a standard tool for assessing both slow and fast HRV dynamics. Fast HRV metrics are commonly derived from the time series of differences between successive intervals ($\Delta RR_i = RR_{i+1} - RR_i$), suggesting a natural extension: a second-order Poincaré plot that captures the temporal structure of ΔRR by plotting ΔRR_i against ΔRR_{i+1}. Our enhanced method introduces these second-order Poincaré plots to uncover higher-order HRV dynamics. We validated this approach on a PhysioNet dataset of 20 healthy individuals. Continuous representations of RR and ΔRR were generated via spline interpolation of discrete interval data to enable cross-spectral analysis of correlations between HRV parameters and respiration. We also developed a coupled-oscillator model to simulate respiratory modulation of heart rate. In contrast to traditional Poincaré plots, which often exhibit elliptical patterns reflecting slow HRV, our method filters out these patterns to emphasize rapid variability. Ring-shaped patterns were found in several participants, showing synchronization between heart rate and respiratory cycles. The plots further revealed distinct serial correlation patterns for g ΔRR_i versus ΔRR_{i+1} across individuals, with positive correlations linked to slow breathing and negative correlations to rapid breathing, and the ratio of respiratory frequency to heart rate serving as the pivotal factor. Our coupled-oscillator model, comprising a fast cardiac integrate-and-fire oscillator modulated by a slower respiratory sinusoid, corroborated these observations. As

such, second-order Poincaré plots offer a powerful tool for dissecting complex HRV dynamics.

Key points

- Second-order Poincaré plots, plotting successive differences of RR intervals (ΔRR_i vs. ΔRR_{i+1}), extend traditional Poincaré analysis to reveal rapid HRV dynamics.
- In a dataset of 20 healthy individuals, second-order plots filtered out slow HRV components, highlighting respiratory modulation.
- Ring-shaped patterns in some participants indicated strong cardiorespiratory coupling, while others showed positive or negative serial correlations linked to breathing rate.
- A coupled-oscillator model confirmed that the ratio of respiratory to heart rate frequency determines serial correlation patterns.
- This method offers a novel tool for analyzing HRV dynamics, with potential applications in physiological and clinical research.

Introduction

Heart rate variability (HRV) captures the interplay between sympathetic and parasympathetic nervous system activity, providing insights into the heart's adaptability to physiological and psychological demands (Shaffer & Ginsberg, 2017). As a non-invasive biomarker, HRV is widely used to evaluate cardiovascular health (Grässler et al., 2021), stress responses (Kim et al., 2018), and emotional regulation (Lane et al., 2009). Clinically, reduced HRV is consistently associated with adverse health outcomes (Lombardi, 2002), and its utility extends beyond cardiology to mental health research, where it serves as a valuable indicator (Kemp & Quintana, 2013). The rise of wearable technology has advanced HRV monitoring, enabling continuous, real-time data collection that enhances clinical diagnostics and personal wellness applications (Dalmeida & Masala, 2021; Li et al., 2023).

HRV analysis employs a range of methodologies, including time-domain and frequency-domain techniques, each offering distinct insights into autonomic nervous system regulation (Shaffer & Ginsberg, 2017). These methods assess autonomic function across various temporal scales, with the fastest fluctuations captured by analyzing consecutive heartbeat intervals, or RR intervals (Calabrese & Lambert-Lacroix, 2025; Tateno & Glass, 2001; Tsipouras et al., 2005). Key parameters for quantifying variability of consecutive RR intervals include the root mean square of successive differences (RMSSD) (Ciccone et al., 2017; Munoz et al., 2015) and the count of interval pairs differing by more than a specified threshold, such as 50 ms (NN50) (Mietus et al., 2002).

A Poincaré plot visualizes heart rate variability (HRV) by plotting each RR interval against the subsequent one ($x = RR_i$, $y = RR_{i+1}$). Initially applied by Raetz et al. (1991) to study RR interval correlations across sleep-wake states in cats, this method revealed distinct heartbeat patterns linked to physiological conditions. Since then, Poincaré plot analysis has become a standard tool for HRV assessment (Khandoker et al., 2013). Its characteristic elliptical point distribution yields two key parameters: SD1, which measures perpendicular

dispersion and reflects parasympathetic-mediated short-term beat-to-beat variability, and SD2, which captures longitudinal dispersion and indicates combined sympathetic and parasympathetic influences on longer-term heart rate dynamics (Brennan et al., 2002; Tulppo et al., 1996; Voss et al., 2009). These metrics together offer a robust assessment of autonomic nervous system control over cardiac function.

This study advances Poincaré analysis by introducing second-order Poincaré plots, providing deeper insights into HRV dynamics. Unlike traditional first-order plots, which map consecutive RR intervals (RR_i vs. RR_{i+1}), this method examines successive interval differences (ΔRR_i vs. ΔRR_{i+1}). Applied to simultaneous electrocardiographic (ECG) and respiratory data from 20 healthy individuals, this approach revealed distinct, respiration-modulated HRV patterns unique to each subject. To elucidate these findings, we used a simple coupled oscillator model, where a rapid cardiac rhythm is dynamically modulated by a slower respiratory rhythm.

Methods

Data source and ethical considerations

This study utilized data from the PhysioNet (Goldberger et al., 2000) dataset “Combined Measurement of ECG, Breathing, and Seismocardiograms Database”, contributed by Miguel Angel Garcia Gonzalez and Ariadna Argelagos Palou at Universitat Politècnica de Catalunya (García-González et al., 2013). The dataset includes recordings from 20 presumed healthy individuals, collected to address two main objectives: first, to examine whether subtle errors in RR interval detection across two ECG leads are influenced by respiratory activity; and second, to compare RR intervals from standard ECG measurements with surrogate estimates derived from seismocardiograms (SCG) to optimize SCG beat-detection algorithms. Data were acquired using a Biopac MP36 system (Santa Barbara, CA, USA), with two channels recording ECG (0.05–150 Hz bandwidth), a third channel capturing respiratory signals via a thoracic piezoresistive band (Biopac SS5LB sensor, 0.05–10 Hz bandwidth), and a fourth channel recording SCG signals using a triaxial accelerometer (LIS344ALH, ST Microelectronics, 0.5–100 Hz bandwidth). ECG electrodes (3M Red Dot 2560) with foam tape and conductive gel were used, and all signals were sampled at 5 kHz. Recordings were conducted with participants awake and motionless in a supine position on a standard bed. After sensor placement, a 5-min baseline recording was obtained, followed by approximately 50 min of classical music listening and a final 5-min rest period.

As the data were publicly available and de-identified, no additional ethical approval was required.

Signal processing

In this study, we analyzed the longest 50-minute music-listening epochs from the dataset, ensuring sufficient data for robust analysis. Signal processing and computations were performed using custom scripts in GNU Octave. The analysis commenced with the selection of the best-quality ECG channel for each participant (Fig. 1A). Following R-peak detection

and timestamping, we processed sequences of four consecutive peaks (t_i, t_{i+1}, t_{i+2}, t_{i+3}) to compute successive RR intervals (RR_i, RR_{i+1}) and their differences (ΔRR_i, ΔRR_{i+1}). These metrics were then used to generate traditional Poincaré plots (RR_i vs. RR_{i+1}; Fig. 1B) and novel second-order Poincaré plots (ΔRR_i vs. ΔRR_{i+1}; Fig. 1C), enabling detailed exploration of heart rate variability dynamics. For the second-order Poincaré plots, we computed the serial correlation coefficient, defined as Pearson's correlation between ΔRR_i and ΔRR_{i+1}.

RR intervals (ΔRR), computed as the difference between successive R-peak timestamps (t_i, t_{i+1}), were assigned a timestamp at the midpoint between them: $(t_i + t_{i+1})/2$. Similarly, the difference of successive RR intervals (ΔRR) was assigned a timestamp at the center weight of the three relevant R-peaks: $(t_i + t_{i+1} + t_{i+2})/3$. These discrete RR and ΔRR time series were then converted into continuous functions of time, RR(t) and $\Delta RR(t)$ using cubic spline interpolation (function interp1) and resampled at 5 kHz to match the original ECG and respiratory signals. This enabled direct comparison and the calculation of cross-spectral densities. For cross-spectral analysis (function cpsd), the continuous signals were downsampled to 5 Hz to focus on the respiratory frequency band (~0.3 Hz). Separately, to analyze the heart rate near ~1 Hz, ECG was downsampled to 50 Hz before computing its power spectral density.

Coupled-oscillator model

We developed a simple coupled-oscillators model to simulate respiratory modulation of heart rate. The cardiac oscillator was implemented as an integrate-and-fire process. Its voltage rose at a rate equal to the inverse of the desired heart rate, and a spike was generated once it reached a fixed threshold. This baseline threshold was calibrated to produce the target heart rate in the absence of other inputs. To simulate physiological variability, we added noise to the threshold and a sinusoidal modulation at the respiratory frequency. As the model was designed for illustrative purposes, its parameter space was not exhaustively explored.

Use of artificial intelligence

Artificial intelligence (AI) was used for language editing. No new material was created using AI. The tool employed was Grok (version 3; xAI, Culver City, CA, USA).

Statistical analysis

Pearson's correlation coefficient, r, was calculated to evaluate serial correlations in second-order Poincaré plots, specifically between ΔRR_i and ΔRR_{i+1}. The significance of r was tested using a t-test. Linear regression was used to analyze the relationship between the modulation frequency-to-heart rate ratio and the ΔRR serial correlation coefficient, r. The model, $y = ax + b$, where a is the slope and b is the intercept, was fitted using the least-squares method. A t-test assessed the significance for this regression. The analyses were performed in GNU Octave.

Results

Figure 2 presents the analysis for three participants from the dataset. A representative 5-minute interval is shown, taken from the 50-minute recording session. For each participant, recordings of respiration are shown and the corresponding values of RR and ΔRR as a function of time (Fig. 2A, C, E). Notably, participant 9 had an unusually low respiratory frequency (approximately 4 breaths per minute), visibly correlated with both RR and ΔRR (Fig. 2C). By contrast, in participants 3 (Fig. 2A) and 19 (Fig. 2E), breath frequencies were approximately 17 and 20 breaths per minute. In all participants, the plots for RR contain very slow heart rate fluctuations (0.01 – 0.1 Hz), which are filtered out when transitioning to ΔRR. In the classical Poincaré plots (Fig. 2B, D, F, top), a characteristic ellipse is present which corresponds to these slow fluctuations, with its major axis aligned along the line y = x. The second-order Poincaré plots (Fig. 2B, D, F, bottom) show additional patterns not evident in the first-order plots. Notably, the second-order plot for participant 3 (Fig. 2B, bottom) very clearly exhibits a ring-like structure, and a ring pattern can be also noticed for participant 19 (Fig. 2F, bottom). This feature is absent in participant 9 (Fig. 2D, bottom). The coefficient of serial correlation, r, is indicated for each second-order Poincaré plot: -0.03, 0.48, and -0.34, for participants 3, 9 and 19, respectively. These values match the orientation of the scatter patterns: for participant 9 (Fig. 2D, bottom), the points cluster along the line y = x (i.e. positive serial correlation) whereas for participant 19 (Fig. 2F, bottom) the point distribution is perpendicular to the line y = x (i.e. negative serial correlation). Importantly, none of these distinct patterns could have been anticipated from the first-order Poincaré plots alone.

The ring-like pattern observed in the second-order Poincaré plot for participants 3 and 19, as well as in five other participants upon visual inspection, suggested that the respiratory cycle might be the primary driver of this effect. To investigate this possibility, we examined the modulations of RR intervals and their changes, ΔRR, in relation to recorded breath patterns. Figure 3 presents the analysis for the same participants as in Fig.2, with respiratory recordings aligned to peak inhalation at the top of panels A, B, and C. The corresponding traces for RR intervals and ΔRR are displayed in the middle and bottom sections of these panels, respectively. To facilitate comparison, the discrete data points derived from R peaks were converted into a continuous representation through interpolation. Breath cycles are clearly correlated with the modulations of RR and ΔRR in all three participants. Additionally, panels D-F in Fig. 3 illustrate the second-order Poincaré plots as three-dimensional visualizations, with time represented along the z-axis. The plots form spirals for participants 3 (Fig. 3D) and 19 (Fig. 3F), with each full rotation corresponding to a complete respiratory cycle. No such spirals are visible for participant 9 (Fig. 3E), which corresponds to the absence of the ring-like pattern for this participant (Fig. 2D, bottom). To confirm the correlation of ΔRR modulations with breathing, cross-spectra (black lines) were computed for respiration versus ΔRR, where the latter was treated as a continuous variable. The spectra for both respiration (green lines) and ΔRR (magenta lines) were also calculated. For participants 3, 9, and 19, this approach clearly identified spectral peaks corresponding to respiratory cycles (Fig. 3G-I). Spectral analyses were similarly performed on ECG records, revealing peaks associated with heart rate at around 1 Hz (Fig. 3J-L).

Additional examples of the second-order Poincaré plots and the corresponding spectra are depicted in Figs 4, 5, and 6, corresponding to ring patterns, positive serial correlation, and

negative serial correlation, respectively. In these illustrated cases (and the other cases that are not shown), peaks are present in the cross-spectra for ΔRR versus respiration at 0.2-0.4 Hz, which reflect cardiorespiratory modulations, and the frequency of 0.075 Hz for subject 9 is unusually low (Fig. 3H). Peaks at the same frequencies are present in the spectra for ΔRR and respiration. In one illustrated case (Fig. 6B), low-frequency drifts are noticeable in the respiratory spectrum, reflecting imperfections of the recordings. Additionally, respiratory spectra are sometimes broad (Figs 5E and 6E) because of the variations in breath frequency. Additionally, ΔRR autospectra in some cases exhibit modulatory frequencies higher than the breath frequency (Figs 5E and 6E). While a detailed analysis of these cases is beyond the scope of this study, they may warrant further investigation, particularly in clinical applications.

To summarize the results obtained thus far, we found that second-order Poincaré plots provided additional insights compared to first-order plots. These plots highlighted rapid modulations of RR intervals, contrasting with the slow modulations captured by the first-order plot ellipse. In some cases, they also revealed ring-like patterns associated with a strong correlation between ΔRR and breath cycles. (But a strong correlation did not necessarily translate to a ring pattern as shown in Figs 2C,D and 3B,E,H.) Additionally, second-order Poincaré plots exposed either positive or negative serial correlations which could not be predicted from the first-order plots.

We analyzed the individual variability in serial correlation in more detail. First, we noticed a trend for the lower breath rates to coincide with positive serial correlation and for the higher breath rates to align with negative serial correlation. Thus, participant 9 exhibited positive serial correlation ($r = 0.48$; Fig. 2D) alongside a very low breath rate (0.075 Hz, Fig. 3H), whereas participant 19 showed negative serial correlation ($r = -0.34$; Fig. 2F) with a higher breath rate (0.35 Hz; Fig. 3I). Second, we noticed that the heart rate also contributed to the serial correlation patterns. Thus, participants 16, and 18 displayed positive serial correlations with a low breath-ΔRR coupling frequency of 0.2 Hz and a somewhat elevated heart rate of 1.3-1.4 Hz (Fig.5).

Next, we considered the interaction between a high-frequency cardiac oscillator (generating pulses roughly every 1 s) and a low-frequency respiratory oscillator (whose cycle spans approximately 3 heartbeats), where altering the rate of either oscillator changes the number of RR intervals within each respiratory cycle. If the respiratory rate slows—and/or the heart rate increases—more RR intervals will fit into a single breath cycle. In such cases, ΔRR tends to follow a pattern where it increases (or decreases) progressively over the course of the respiratory cycle, leading to a positive serial correlation in ΔRR. Conversely, if the respiratory rate increases—and/or the heart rate decreases—fewer RR intervals occur within each breath cycle. As a result, the respiratory cycle becomes too short to sustain a consistent directional change in ΔRR, causing fluctuations that instead produce a negative serial correlation.

To verify whether this mechanism applied to our data, we examined the relationship between the breath-to-heart rate ratio (a measure proportional to the number of RR intervals per respiratory cycle) and the ΔRR serial correlation coefficient, as shown in Fig. 7. The figure presents two variants of this analysis. Figure 7A uses the respiratory frequency derived from cross-spectral analysis (representing the frequency at which respiration modulates ΔRR),

while Figure 7B uses the dominant modulation frequency obtained from the ΔRR spectrum. As noted earlier, these frequencies typically coincided when respiratory modulation of heart rate was strong. However, discrepancies arose in certain cases due to additional non-respiratory heart rate modulations (e.g., Figs 5E and 6E) or questionable respiratory signal quality (e.g. Fig. 6B). This justified the inclusion of Fig. 7B's analysis, which becomes particularly relevant when respiratory recordings are unavailable. Additionally, with long analysis epochs (such as 5 minutes in Figs 2-6), nonstationarities could occur in both breath and heart patterns, altering the results of these analyses. Therefore, for both analyses, the 50-min recordings were segmented into 100-second epochs (yielding 60 epochs per participant). Regression analysis confirmed our hypothesis in both cases, though the fit was stronger when using the modulation frequency derived solely from the ΔRR spectrum.

To further verify the proposed mechanism of negative versus serial correlation in ΔRR for different breathing and heart rates, we developed a simple model of the coupling between an approximately 1 Hz cardiac oscillator with an approximately 0.3 Hz respiratory oscillator (Fig. 8). The cardiac oscillator was modeled using an integrate-and-fire mechanism with a constant rate of rise but a randomly fluctuating starting point (Fig. 8A). An impulse was generated when the integrated rate reached a threshold that was sinusoidally modulated according to the breathing rate. The model successfully reproduced the expected relationship between the ratio of respiration rate to heart rate, which was accurately described by a linear fit (Fig. 8B). Figure 8C displays second-order Poincaré plots for different model parameters, illustrating a transition from positive to negative serial correlation as breathing rate increased and/or heart rate decreased. Intermediate parameter settings also revealed distinct ring-like patterns, further supporting the model's ability to capture the observed dynamics.

Discussion

The present findings build upon the classical Poincaré analysis of HRV, as established in prior research (Brennan et al. 2002; Kamen et al. 1996; Khandoker et al. 2013; Raetz et al. 1991; Tulppo et al. 1996; Voss et al. 2009), by introducing a second-order Poincaré plot in which ΔRR_i is plotted against ΔRR_{i+1}. This extension aligns naturally with the existing framework, given that interpretations of Poincaré plots are fundamentally rooted in the statistical properties of ΔRR. The visualization and quantification of serial dependencies in ΔRR thus provide a coherent and meaningful advancement of the methodology.

In the present study, the introduction of the second-order Poincaré plot improved the analysis of cardiorespiratory coupling—the physiological interplay between breathing rhythms and heart rate modulation. Respiration influences cardiac activity through well-established neural mechanisms, particularly respiratory sinus arrhythmia, characterized by heart rate acceleration during inspiration and deceleration during expiration (Berntson et al., 1993; Larsen et al., 2010; Yasuma & Hayano, 2004). Analysis of individual data revealed distinct coupling patterns, with some participants exhibiting pronounced ring-like structures in the second-order Poincaré plots, while others displayed varying degrees of serial correlation in ΔRR intervals. Cross-spectral analysis confirmed respiratory modulation in all cases. We proposed that breathing frequency relative to heart rate determines the observed individual differences: slower respiration produces sustained directional changes in successive RR

intervals, yielding positive serial correlations, whereas faster breathing induces more frequent reversals in interval dynamics, leading to negative correlations. This hypothesis was tested using a simple integrate-and-fire oscillator model, where respiration modulated threshold crossings. This model supported the notion that respiratory frequency shaped the temporal structure of HRV, as captured by second-order Poincaré analysis.

Here we analyzed a single data set—the recordings from healthy individuals lying quietly in bed and listening to music. Under these conditions, respiratory modulation of heart rate is likely to be especially prominent. It would be informative to extend our analysis to other conditions in which first-order Poincaré analysis has been applied previously, for example heart-rate recordings during different breathing regimes (Guzik et al. 2005; 2007), during exercise (Mourot et al. 2004), and in studies of autonomic influences such as head tilts and pharmacological agents (Kamen et al. 1996; Karmakar et al. 2011). It would also be of interest to determine whether second-order Poincaré plots offer additional utility for clinical cases like arrhythmias, where first-order analysis has already been used (Zhang et al. 2015).

In conclusion, our results underscore the value of second-order Poincaré analysis for uncovering dynamical features that conventional HRV metrics may miss. Future research should examine whether similar patterns occur in other physiological oscillator systems and how these dynamics change across different physiological and cognitive conditions, disease states, or pharmacological interventions. The potential clinical applications warrant further exploration, particularly for conditions involving autonomic dysfunction or impaired cardiorespiratory coupling.

Conclusions

The present study extends classical Poincaré analysis by introducing a second-order Poincaré plot, where ΔRR_i is plotted against ΔRR_{i+1}. This approach aligns naturally with the statistical foundations of traditional Poincaré analysis and provides a coherent methodological advancement by explicitly visualizing and quantifying serial dependencies in ΔRR. Our findings demonstrate that this technique enhances the analysis of cardiorespiratory coupling, revealing individual-specific patterns—such as ring-like structures and distinct serial correlations in ΔRR—that reflect the influence of respiration on heart rate modulation. Cross-spectral analysis confirmed respiratory influences in all participants, and computational modeling supported the hypothesis that respiratory frequency relative to heart rate shapes these dynamics, with slower breathing leading to positive serial correlations and faster breathing producing negative correlations.

While this study focused on healthy individuals at rest, where respiratory modulation is pronounced, the methodology holds promise for broader applications. Future work should explore its utility across diverse physiological states, such as controlled breathing protocols, exercise, autonomic challenges, and clinical conditions including arrhythmias or autonomic dysfunction. Such investigations could clarify whether second-order Poincaré plots offer improved discriminative or prognostic value in these settings. Ultimately, this approach provides a refined tool for uncovering subtle dynamical features in heart rate variability and can contribute to a deeper understanding of complex physiological interactions in both health and disease.

References

Berntson, G. G., Cacioppo, J. T., & Quigley, K. S. (1993). Respiratory sinus arrhythmia: Autonomic origins, physiological mechanisms, and psychophysiological implications. Psychophysiology, 30(2), 183-196.

Brennan, M., Palaniswami, M., & Kamen, P. (2002). Do existing measures of Poincare plot geometry reflect nonlinear features of heart rate variability?. IEEE transactions on biomedical engineering, 48(11), 1342-1347.

Calabrese, P., & Lambert-Lacroix, S. (2025). Inspiratory and expiratory sinus arrhythmia in healthy human. Physiological Reports, 13(7), e70245.

Ciccone, A. B., Siedlik, J. A., Wecht, J. M., Deckert, J. A., Nguyen, N. D., & Weir, J. P. (2017). Reminder: RMSSD and SD1 are identical heart rate variability metrics. Muscle & nerve, 56(4), 674-678.

Dalmeida, K. M., & Masala, G. L. (2021). HRV features as viable physiological markers for stress detection using wearable devices. Sensors, 21(8), 2873.

García-González, M. A., Argelagós-Palau, A., Fernández-Chimeno, M., & Ramos-Castro, J. (2013, September). A comparison of heartbeat detectors for the seismocardiogram. In Computing in Cardiology 2013 (pp. 461-464). IEEE.

Goldberger, A., Amaral, L., Glass, L., Hausdorff, J., Ivanov, P. C., Mark, R., ... & Stanley, H. E. (2000). PhysioBank, PhysioToolkit, and PhysioNet: Components of a new research resource for complex physiologic signals. Circulation [Online]. 101 (23), pp. e215–e220. RRID:SCR_007345.

Grässler, B., Thielmann, B., Böckelmann, I., & Hökelmann, A. (2021). Effects of different exercise interventions on heart rate variability and cardiovascular health factors in older adults: a systematic review. European Review of Aging and Physical Activity, 18(1), 24.

Guzik, P., Piskorski, J., Krauze, T., Schneider, R., Wesseling, K. H., Wykretowicz, A., & Wysocki, H. (2005). The influence of changing respiratory rate on HRV is portrayed by descriptors of Poincaré plot analysis. Folia Cardiol, 12, 17-20.

Guzik, P., Piskorski, J., Krauze, T., Schneider, R., Wesseling, K. H., Wykretowicz, A., & Wysocki, H. (2007). Correlations between the Poincaré plot and conventional heart rate variability parameters assessed during paced breathing. The Journal of Physiological Sciences, 57(1), 63-71.

Kamen, P. W., Krum, H., & Tonkin, A. M. (1996). Poincare plot of heart rate variability allows quantitative display of parasympathetic nervous activity in humans. Clinical science, 91(2), 201-208.

Karmakar, C. K., Khandoker, A. H., Voss, A., & Palaniswami, M. (2011). Sensitivity of temporal heart rate variability in Poincaré plot to changes in parasympathetic nervous system activity. Biomedical engineering online, 10(1), 17.

Kemp, A. H., & Quintana, D. S. (2013). The relationship between mental and physical health: insights from the study of heart rate variability. International journal of Psychophysiology, 89(3), 288-296.

Khandoker, A. H., Karmakar, C., Brennan, M., Palaniswami, M., & Voss, A. (2013). Poincaré plot methods for heart rate variability analysis (pp. 13-23). New York: Springer.

Kim, H. G., Cheon, E. J., Bai, D. S., Lee, Y. H., & Koo, B. H. (2018). Stress and heart rate variability: a meta-analysis and review of the literature. Psychiatry investigation, 15(3), 235.

Lane, R. D., McRae, K., Reiman, E. M., Chen, K., Ahern, G. L., & Thayer, J. F. (2009). Neural correlates of heart rate variability during emotion. Neuroimage, 44(1), 213-222.

Li, K., Cardoso, C., Moctezuma-Ramirez, A., Elgalad, A., & Perin, E. (2023). Heart rate variability measurement through a smart wearable device: another breakthrough for personal health monitoring?. International journal of environmental research and public health, 20(24), 7146.

Lombardi, F. (2002). Clinical implications of present physiological understanding of HRV components. Cardiac electrophysiology review, 6(3), 245-249.

Mietus, J. E., Peng, C. K., Henry, I., Goldsmith, R. L., & Goldberger, A. L. (2002). The pNNx files: re-examining a widely used heart rate variability measure. Heart, 88(4), 378-380.

Mourot, L., Bouhaddi, M., Perrey, S., Cappelle, S., Henriet, M. T., Wolf, J. P., ... & Regnard, J. (2004). Decrease in heart rate variability with overtraining: assessment by the Poincare plot analysis. Clinical physiology and functional imaging, 24(1), 10-18.

Munoz, M. L., Van Roon, A., Riese, H., Thio, C., Oostenbroek, E., Westrik, I., ... & Snieder, H. (2015). Validity of (ultra-) short recordings for heart rate variability measurements. PloS one, 10(9), e0138921.

Larsen, P. D., Tzeng, Y. C., Sin, P. Y. W., & Galletly, D. C. (2010). Respiratory sinus arrhythmia in conscious humans during spontaneous respiration. Respiratory physiology & neurobiology, 174(1-2), 111-118.

Raetz, S. L., Richard, C. A., Garfinkel, A., & Harper, R. M. (1991). Dynamic characteristics of cardiac RR intervals during sleep and waking states. Sleep, 14(6), 526-533.

Shaffer, F., & Ginsberg, J. P. (2017). An overview of heart rate variability metrics and norms. Frontiers in public health, 5, 258.

Tateno, K., & Glass, L. (2001). Automatic detection of atrial fibrillation using the coefficient of variation and density histograms of RR and ΔRR intervals. Medical and Biological Engineering and Computing, 39(6), 664-671.

Tsipouras, M. G., Fotiadis, D. I., & Sideris, D. (2005). An arrhythmia classification system based on the RR-interval signal. Artificial intelligence in medicine, 33(3), 237-250.

Tulppo, M. P., Makikallio, T. H., Takala, T. E., Seppanen, T. H. H. V., & Huikuri, H. V. (1996). Quantitative beat-to-beat analysis of heart rate dynamics during exercise. American journal of physiology-heart and circulatory physiology, 271(1), H244-H252.

Voss, A., Schulz, S., Schroeder, R., Baumert, M., & Caminal, P. (2009). Methods derived from nonlinear dynamics for analysing heart rate variability. Philosophical Transactions of the Royal Society A: Mathematical, Physical and Engineering Sciences, 367(1887), 277-296.

Yasuma, F., & Hayano, J. I. (2004). Respiratory sinus arrhythmia: why does the heartbeat synchronize with respiratory rhythm?. Chest, 125(2), 683-690.

Zhang, L., Guo, T., Xi, B., Fan, Y., Wang, K., Bi, J., & Wang, Y. (2015). Automatic recognition of cardiac arrhythmias based on the geometric patterns of Poincaré plots. Physiological measurement, 36(2), 283.

Additional information

Data availability statement

The experimental data used for this analysis are available online (https://physionet.org/content/cebsdb/1.0.0/), and software will be made fully available upon the completion of the review process.

Competing interests

The authors have no competing interests to declare.

Author contributions

MAL and DFK conceived and designed the study. MAL, ASM, KSP, and DFK analyzed the data. MAL, NMS, AVM and DFK wrote the manuscript. All authors reviewed and approved the final version of the manuscript.

Funding

This study was carried out within the support of the state assignment of the IITP RAS approved by the Ministry of Education and Science of Russia.

Keywords

Heart rate variability, Poincare plot, cardiorespiratory, serial correlation, RR intervals.

Figures

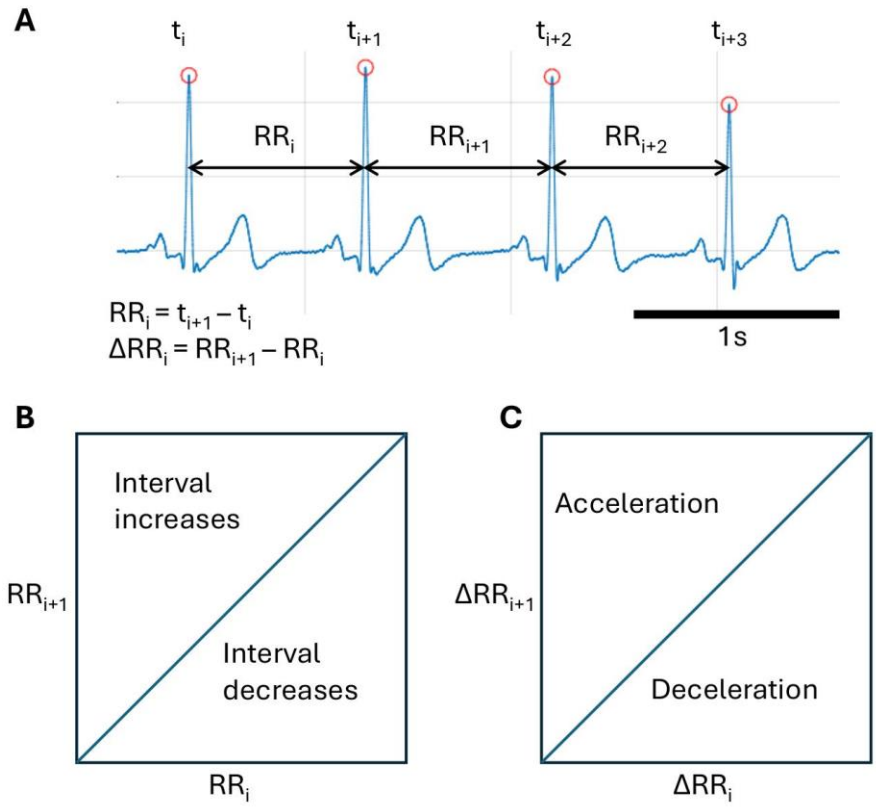

Figure 1. Construction of the first-order and second-order Poincaré plots. A: ECG trace with detected R peaks marked by red circles. Four consecutive peaks are timestamped, and their occurrence times are used to compute RR intervals and successive differences (ΔRR). B: First-order Poincaré plot with RR_i on the x-axis and RR_{i+1} on the y-axis. Points above the line y = x indicate RR interval lengthening, while points below the line indicate shortening. C: Second-order Poincaré plot with ΔRR_i on the x-axis and ΔRR_{i+1} on the y-axis. Points above the line y = x correspond to RR interval acceleration (ΔR increase), while points below the line indicate deceleration (ΔR decrease).

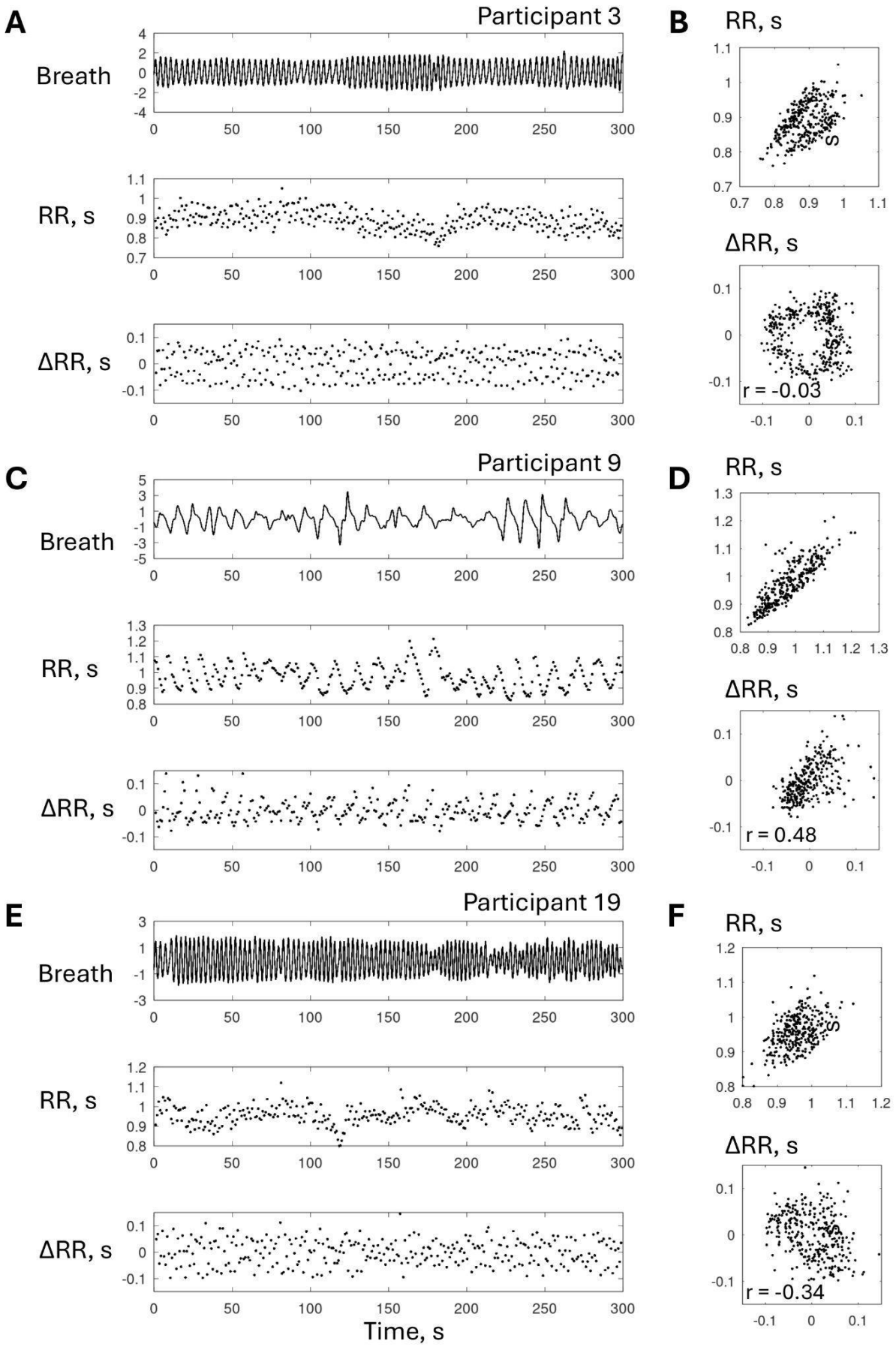
A
Participant 3
Breath
RR, s
ΔRR, s
B
RR, s
ΔRR, s
r = -0.03
C
Participant 9
Breath
RR, s
ΔRR, s
D
RR, s
ΔRR, s
r = 0.48
E
Participant 19
Breath
RR, s
ΔRR, s
Time, s
F
RR, s
ΔRR, s
r = -0.34

Figure 2. Time course of heartbeat intervals (RR) and their changes (ΔRR), along with first-order and second-order Poincaré plots for the same data. A, C, E: Respiration (top), RR (middle) and ΔRR (bottom) plotted over time for participants 3, 9, and 19, respectively. B, D, F: First-order (top) and second-order (bottom) Poincaré plots for the corresponding participants.

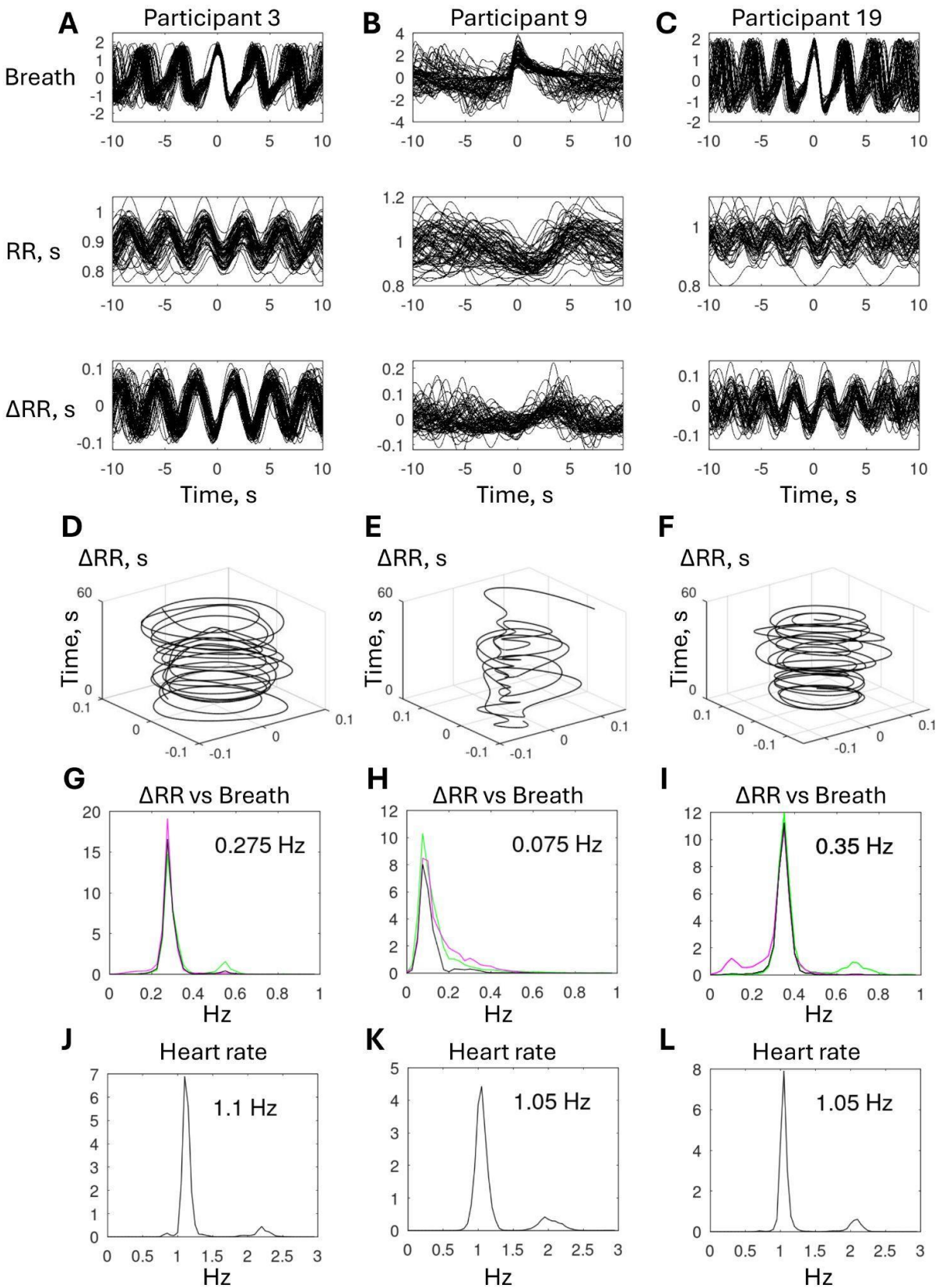

Figure 3. Comparison of respiratory cycles with modulations of RR intervals and ΔRR in participants 3, 9, and 19 (the same as in Fig. 2). RR and ΔRR values were interpolated to generate continuous traces. A-C: Respiratory traces (top) aligned to peak inhalation, with

corresponding RR (middle) and ΔRR (bottom) modulations. D-F: Three-dimensional representations of the second-order Poincaré plots, with time as the third axis. Spiral patterns reflect respiratory cycles in D and F. G-I: Cross-spectral analysis of respiratory-related modulations. Black lines represent cross-spectra (ΔRR vs. respiration), while colored lines denote spectra for respiration (green) and ΔRR (magenta). Frequencies corresponding to the peaks of ΔRR–respiration cross-spectra are indicated. J-L: ECG spectra, with peaks corresponding to heart rate.

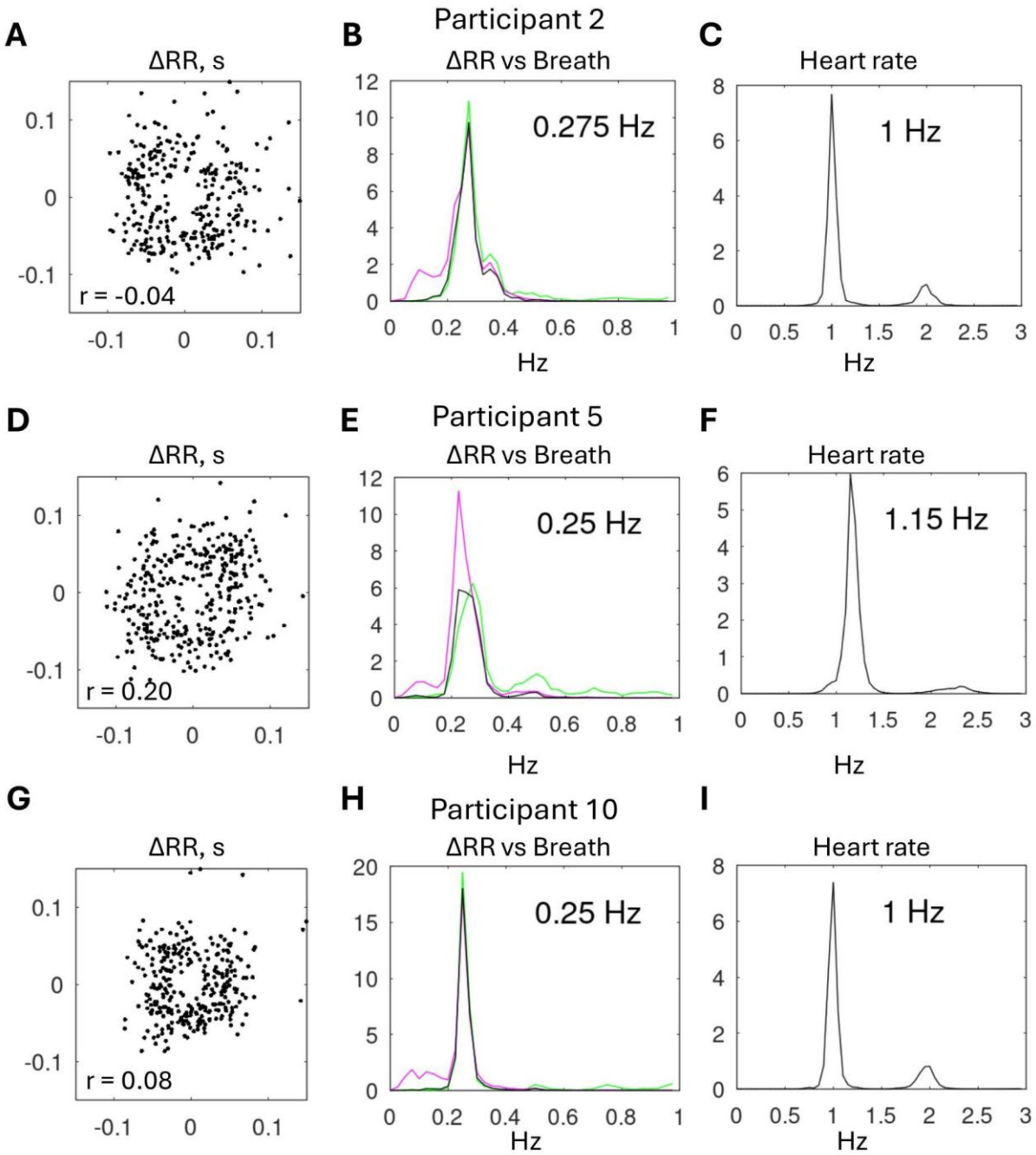

Figure 4. Examples of ring patterns in the second-order Poincaré plots and the corresponding spectra and cross-spectra. Results are shown for 5 minutes of recordings in participants 2, 5, and 10. A, D, G: Second-order Poincaré plots, with the coefficient of serial correlation, r, indicated. B, E, H: Cross-spectral analysis of respiratory-related modulations.

Black lines represent cross-spectra (ΔRR vs. respiration), while colored lines denote spectra for respiration (green) and ΔRR (magenta). Frequencies corresponding to the peaks of ΔRR–respiration cross-spectra are indicated. C, F, I: ECG spectra, with peaks corresponding to heart rate.

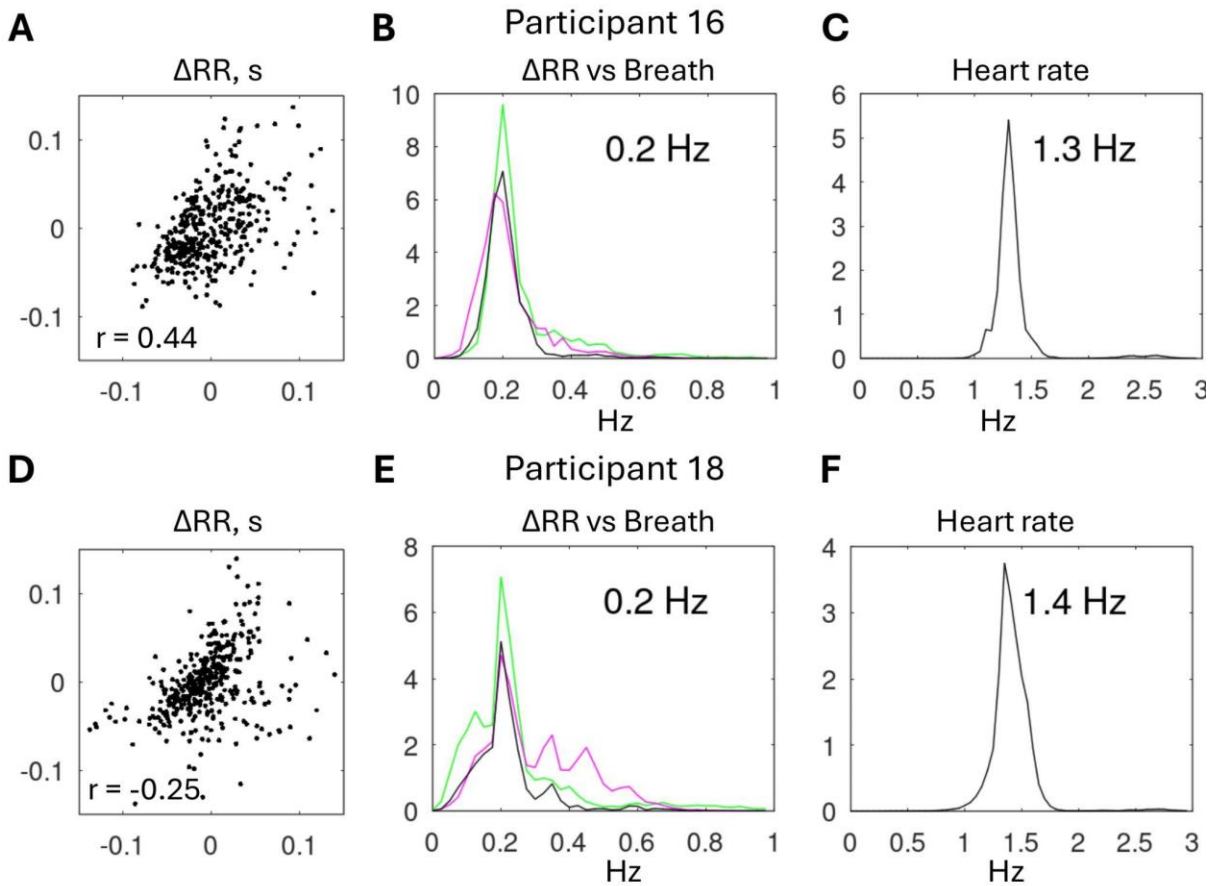

Figure 5. Second-order Poincaré plots and spectral analysis of heart rate versus respiration for two participants (16 and 18) with positive serial correlation for ΔRR. Conventions as in Fig. 4.

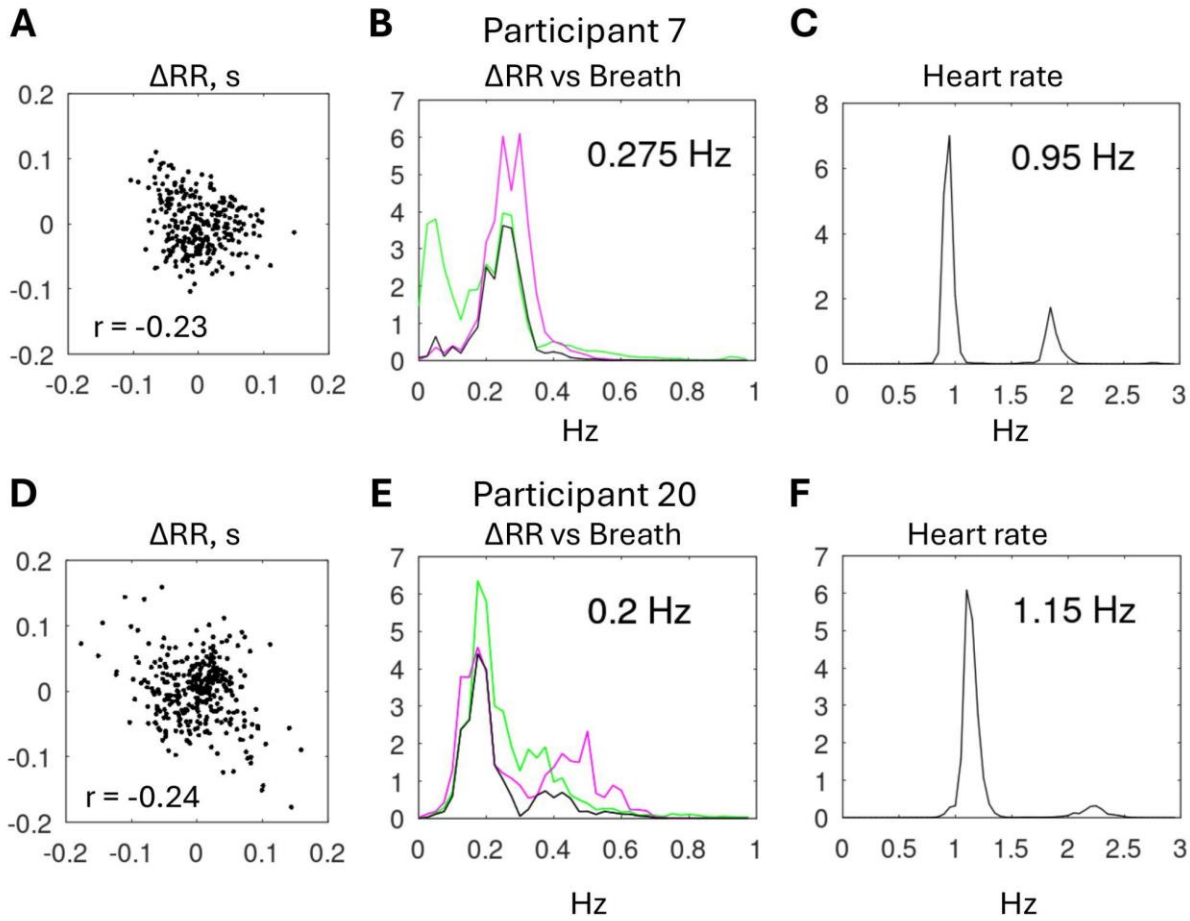

Figure 6. Second-order Poincaré plots and spectral analysis of heart rate versus respiration for two participants (7 and 20) with negative serial correlation for ΔRR. Conventions as in Fig. 4.

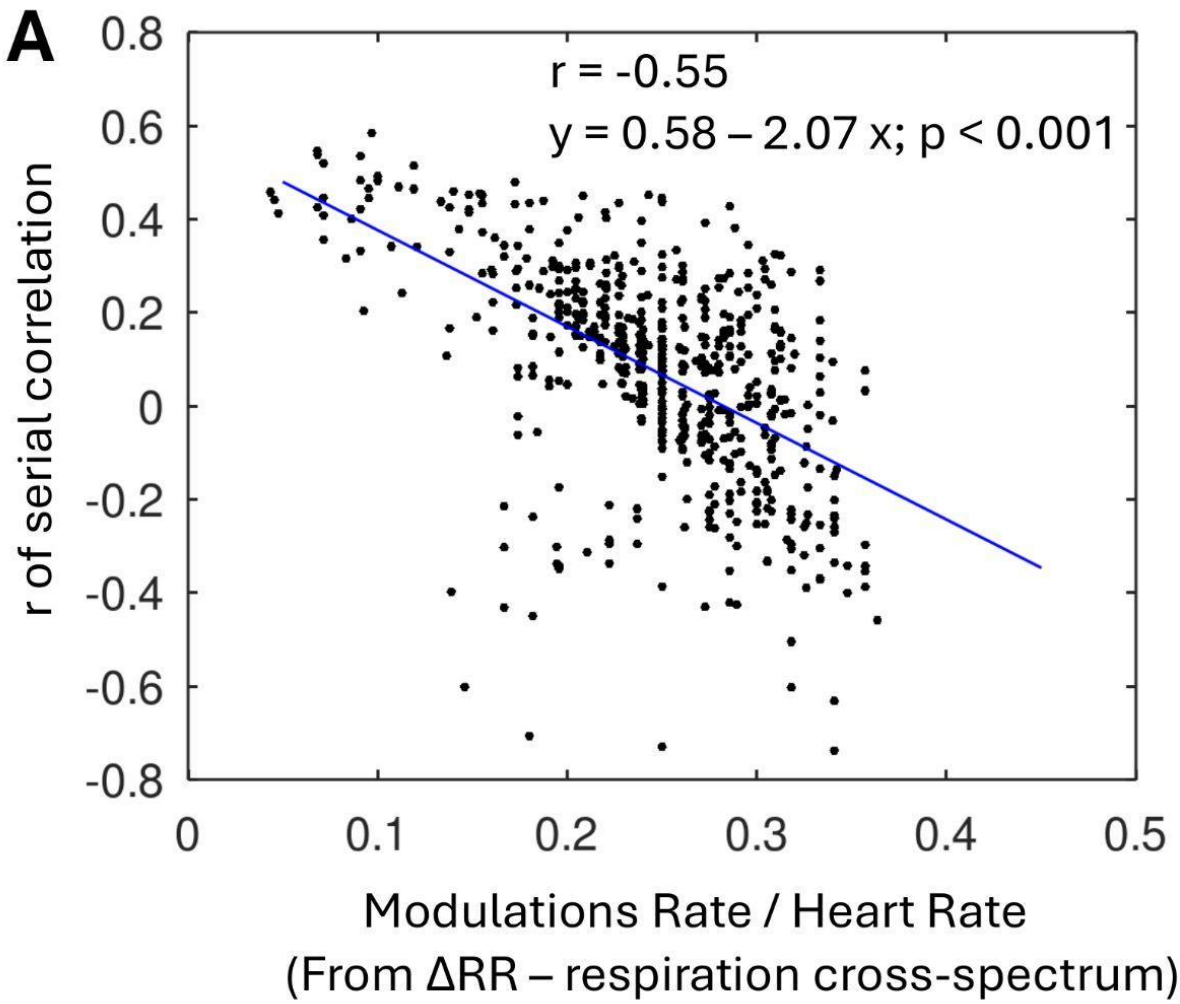
A
r = -0.55
y = 0.58 – 2.07 x; p < 0.001
r of serial correlation
0.8
0.6
0.4
0.2
0
-0.2
-0.4
-0.6
-0.8
0
0.1
0.2
0.3
0.4
0.5
Modulations Rate / Heart Rate
(From ΔRR – respiration cross-spectrum)

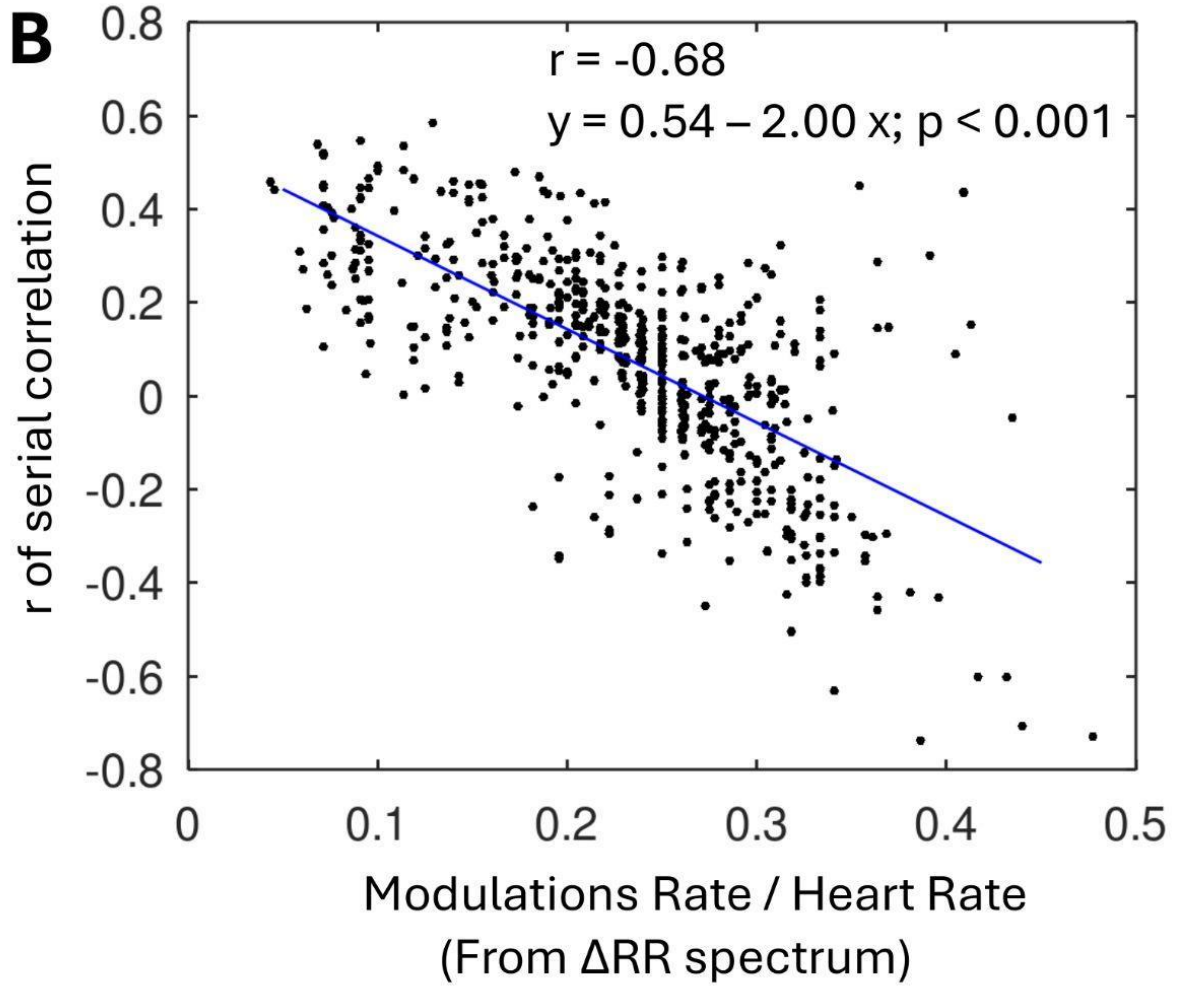
B
r = -0.68
y = 0.54 – 2.00 x; p < 0.001
r of serial correlation
0.8
0.6
0.4
0.2
0
-0.2
-0.4
-0.6
-0.8
0
0.1
0.2
0.3
0.4
0.5
Modulations Rate / Heart Rate
(From ΔRR spectrum)

Figure 7. Relationship between modulation frequency-to-heart rate ratio (x-axis) and ΔRR serial correlation coefficient (y-axis). Each data point represents a 100-s epoch taken from a 50-min recording session. Solid lines show linear regression fits with corresponding equations (y = ax + b), correlation coefficients (r), and p-values indicated. A: Modulation frequency obtained from cross-spectral analysis of respiration and ΔRR.
B: Modulation frequency obtained from spectral analysis of ΔRR alone.

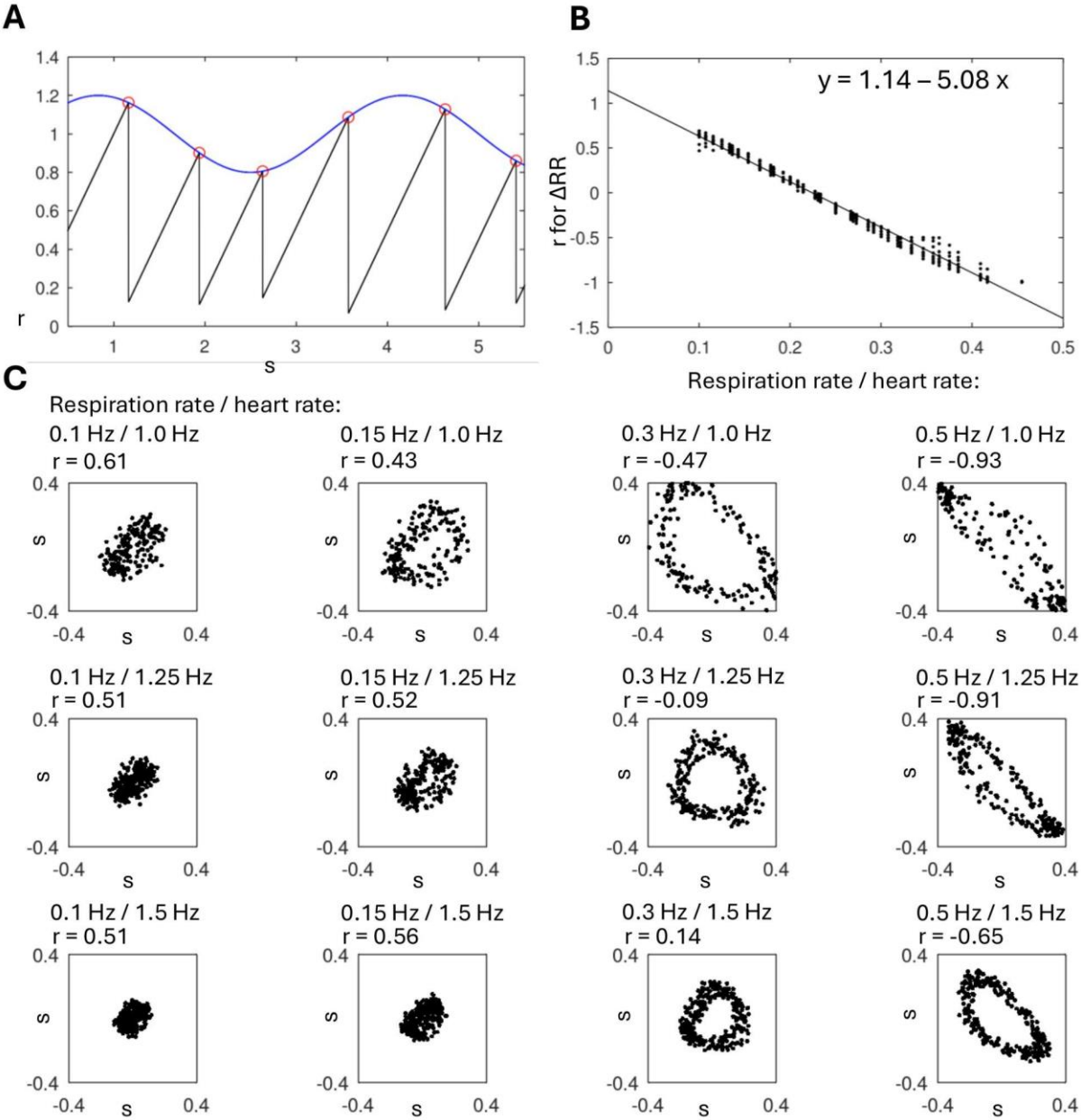

Figure 8. A simple model of coupling between a fast cardiac oscillator (~1 Hz) and a slow respiratory oscillator (~0.3 Hz). A: The cardiac oscillator was modeled as an integrate-and-fire pacemaker with a constant rate of rise but a randomly varying starting point. Impulses were generated when the integrated signal reached a threshold, which was sinusoidally modulated by respiratory activity. B: Linear regression of the respiration-to-heart-rate ratio against the serial correlation coefficient of ΔRR. C: Second-order Poincaré plots illustrating

the shift from positive to negative serial correlation as breathing rate increased and/or heart rate decreased, with ring-like patterns emerging at intermediate parameter values.

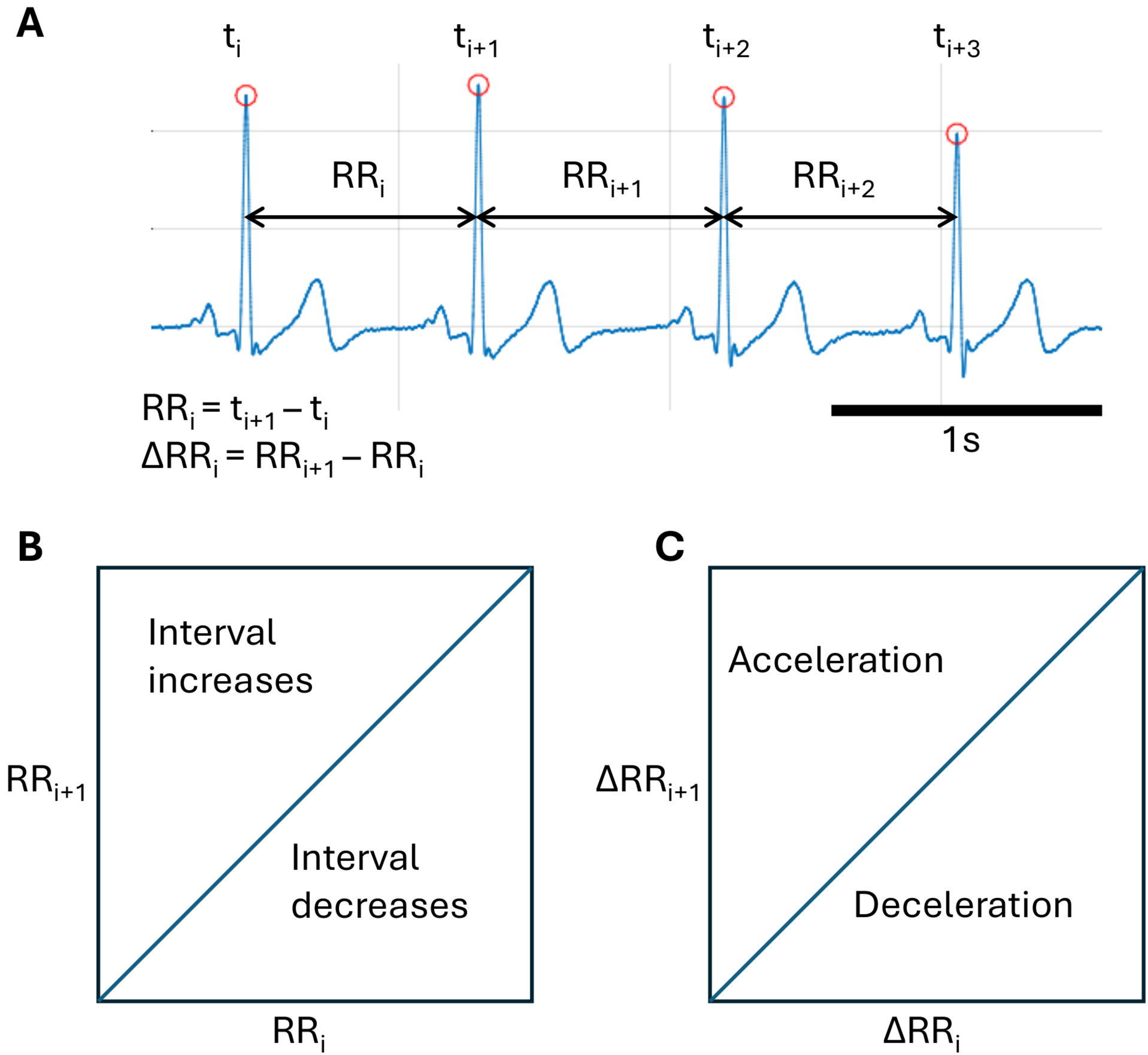
A
t_i
t_{i+1}
t_{i+2}
t_{i+3}
RR_i
RR_{i+1}
RR_{i+2}
$RR_i = t_{i+1} - t_i$
$\Delta RR_i = RR_{i+1} - RR_i$
1s
B
Interval increases
Interval decreases
RR_{i+1}
RR_i
C
Acceleration
Deceleration
ΔRR_{i+1}
ΔRR_i

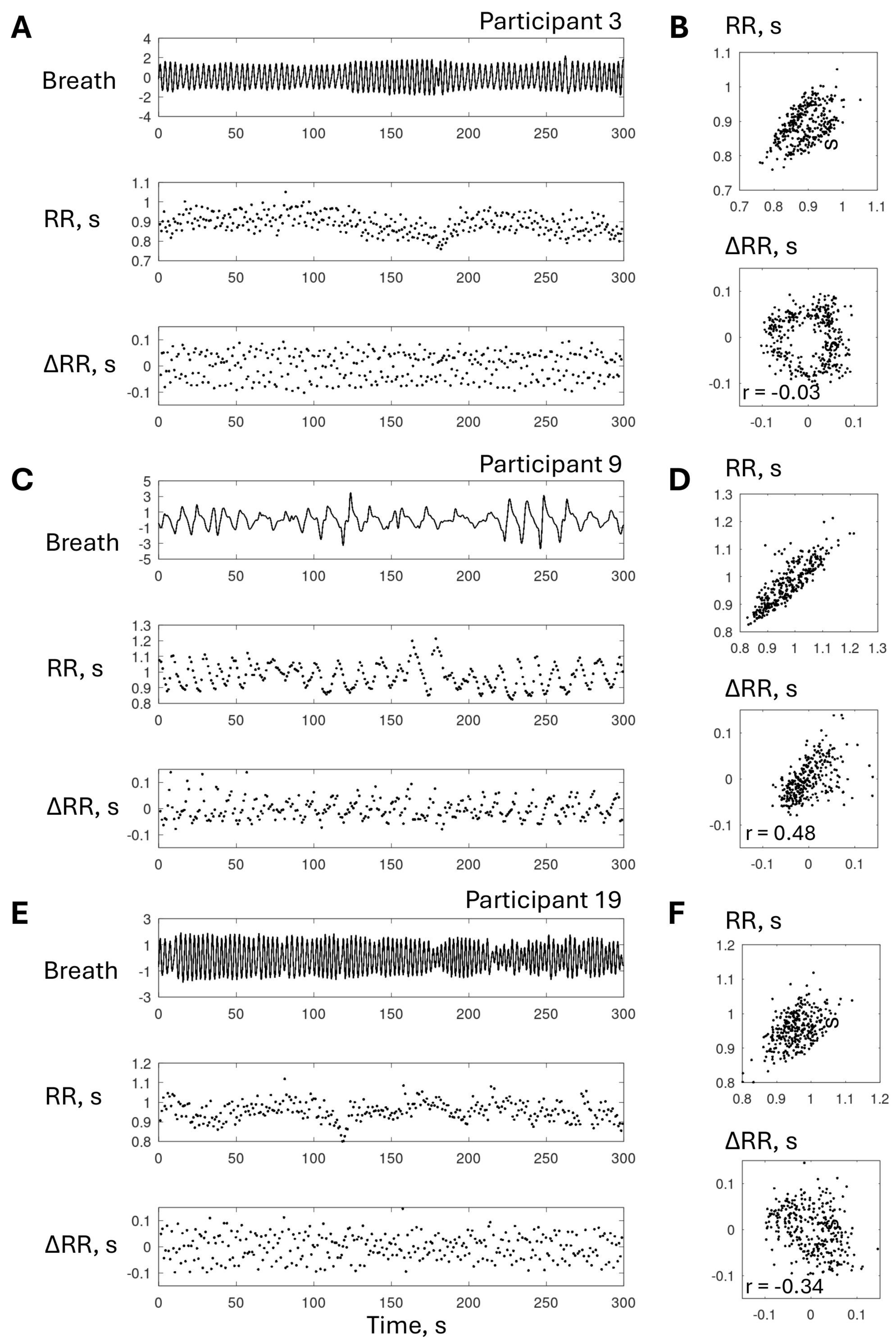
A
Participant 3
Breath
RR, s
ΔRR, s
B
RR, s
ΔRR, s
r = -0.03
C
Participant 9
Breath
RR, s
ΔRR, s
D
RR, s
ΔRR, s
r = 0.48
E
Participant 19
Breath
RR, s
ΔRR, s
Time, s
F
RR, s
ΔRR, s
r = -0.34

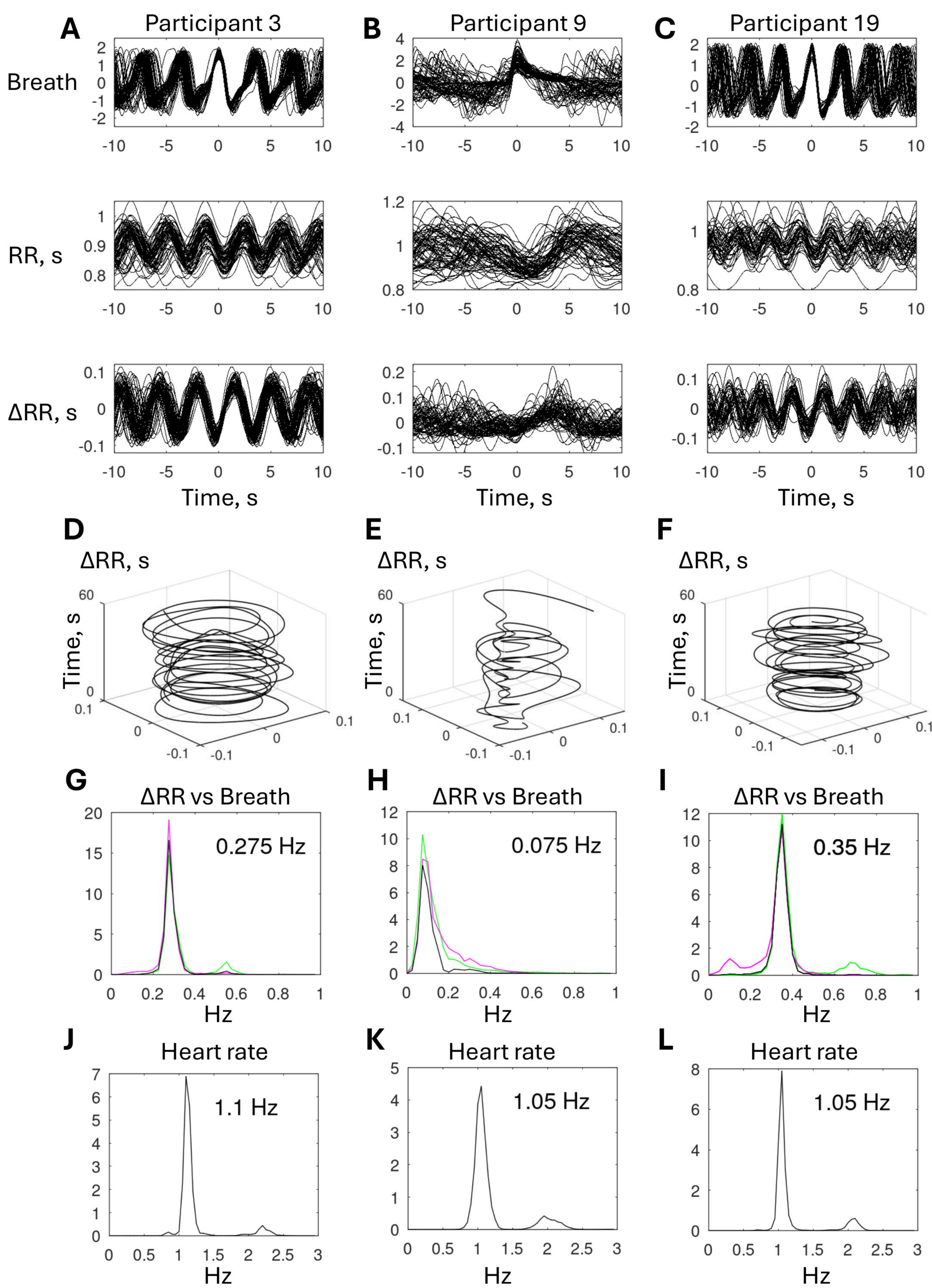
A
Participant 3
B
Participant 9
C
Participant 19
Breath
RR, s
ΔRR, s
Time, s
D
E
F
ΔRR, s
Time, s
G
ΔRR vs Breath
0.275 Hz
H
ΔRR vs Breath
0.075 Hz
I
ΔRR vs Breath
0.35 Hz
Hz
J
Heart rate
1.1 Hz
K
Heart rate
1.05 Hz
L
Heart rate
1.05 Hz
Hz

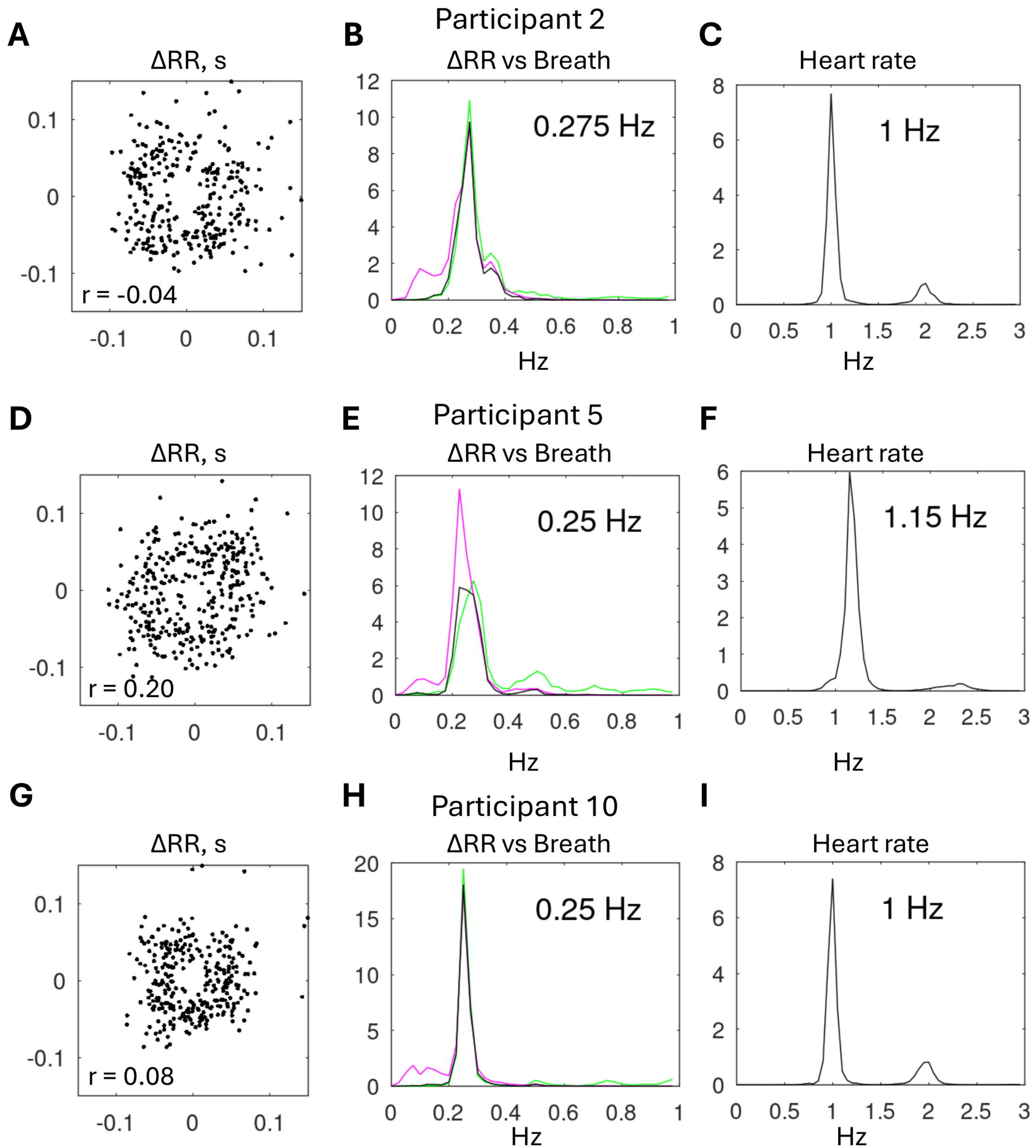
Participant 2
A
ΔRR, s
r = -0.04
B
ΔRR vs Breath
0.275 Hz
Hz
C
Heart rate
1 Hz
Hz
Participant 5
D
ΔRR, s
r = 0.20
E
ΔRR vs Breath
0.25 Hz
Hz
F
Heart rate
1.15 Hz
Hz
Participant 10
G
ΔRR, s
r = 0.08
H
ΔRR vs Breath
0.25 Hz
Hz
I
Heart rate
1 Hz
Hz

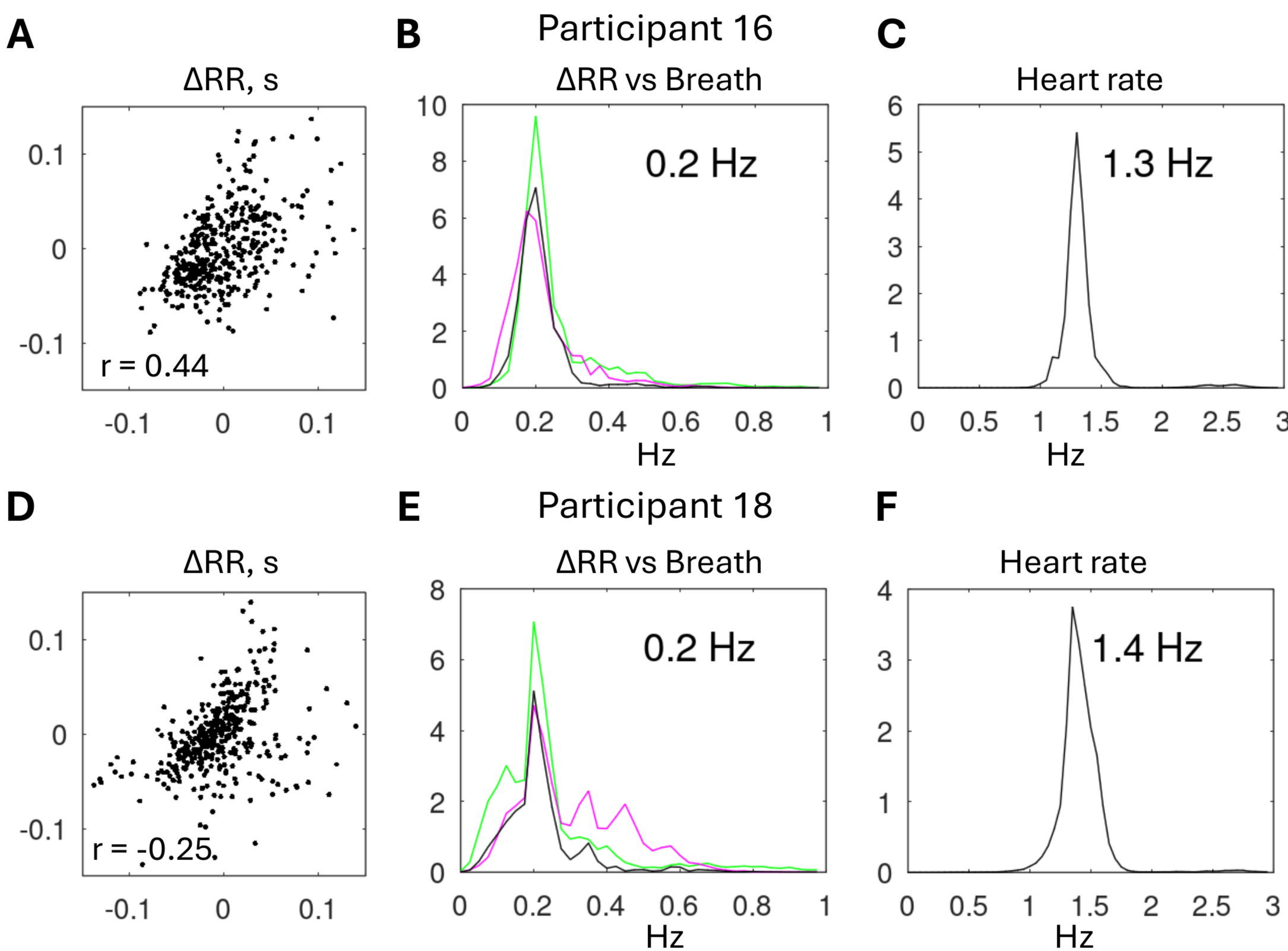
A
ΔRR, s
r = 0.44
B
Participant 16
ΔRR vs Breath
0.2 Hz
Hz
C
Heart rate
1.3 Hz
Hz
D
ΔRR, s
r = -0.25
E
Participant 18
ΔRR vs Breath
0.2 Hz
Hz
F
Heart rate
1.4 Hz
Hz

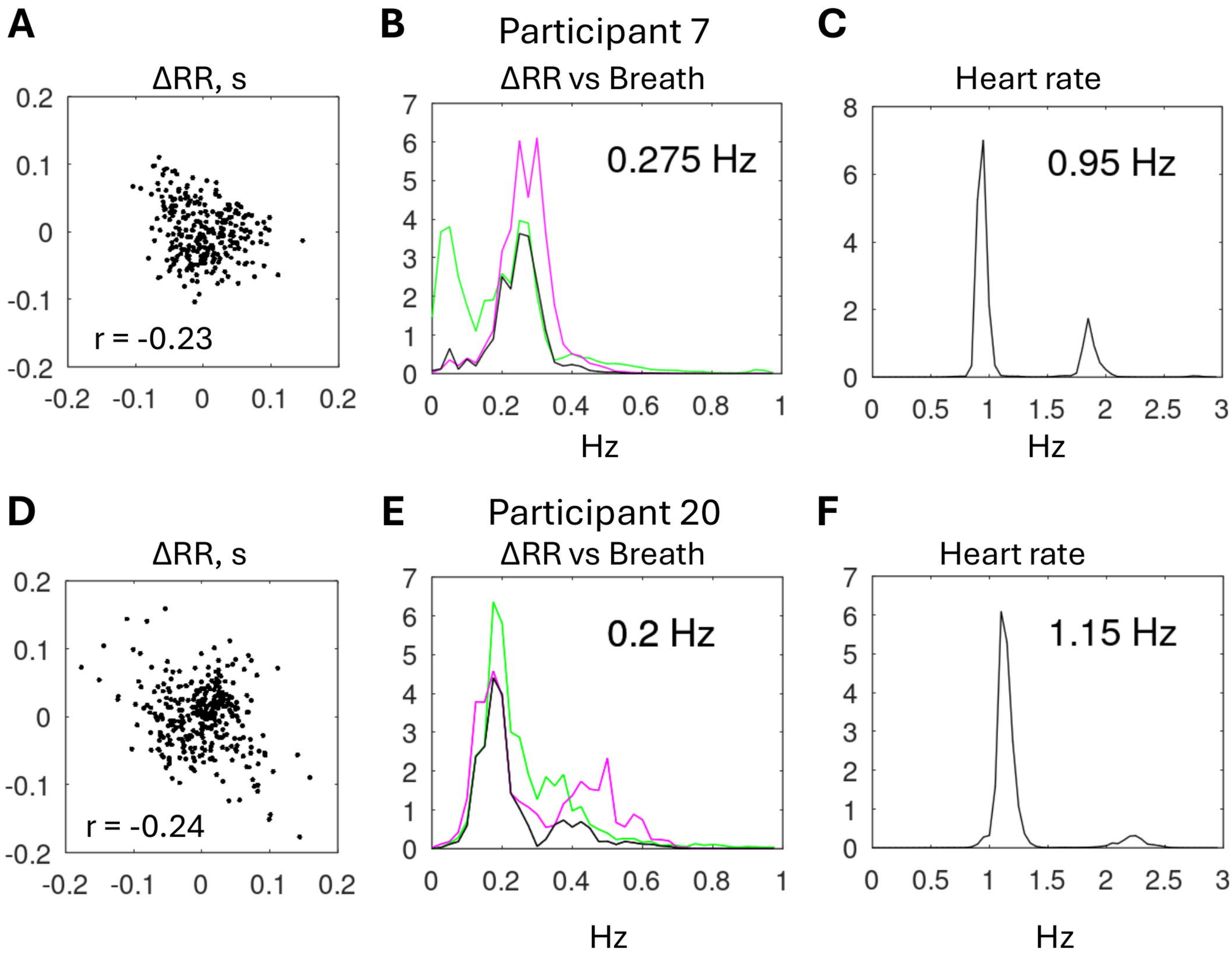
A
ΔRR, s
r = -0.23
B
Participant 7
ΔRR vs Breath
0.275 Hz
Hz
C
Heart rate
0.95 Hz
Hz
D
ΔRR, s
r = -0.24
E
Participant 20
ΔRR vs Breath
0.2 Hz
Hz
F
Heart rate
1.15 Hz
Hz

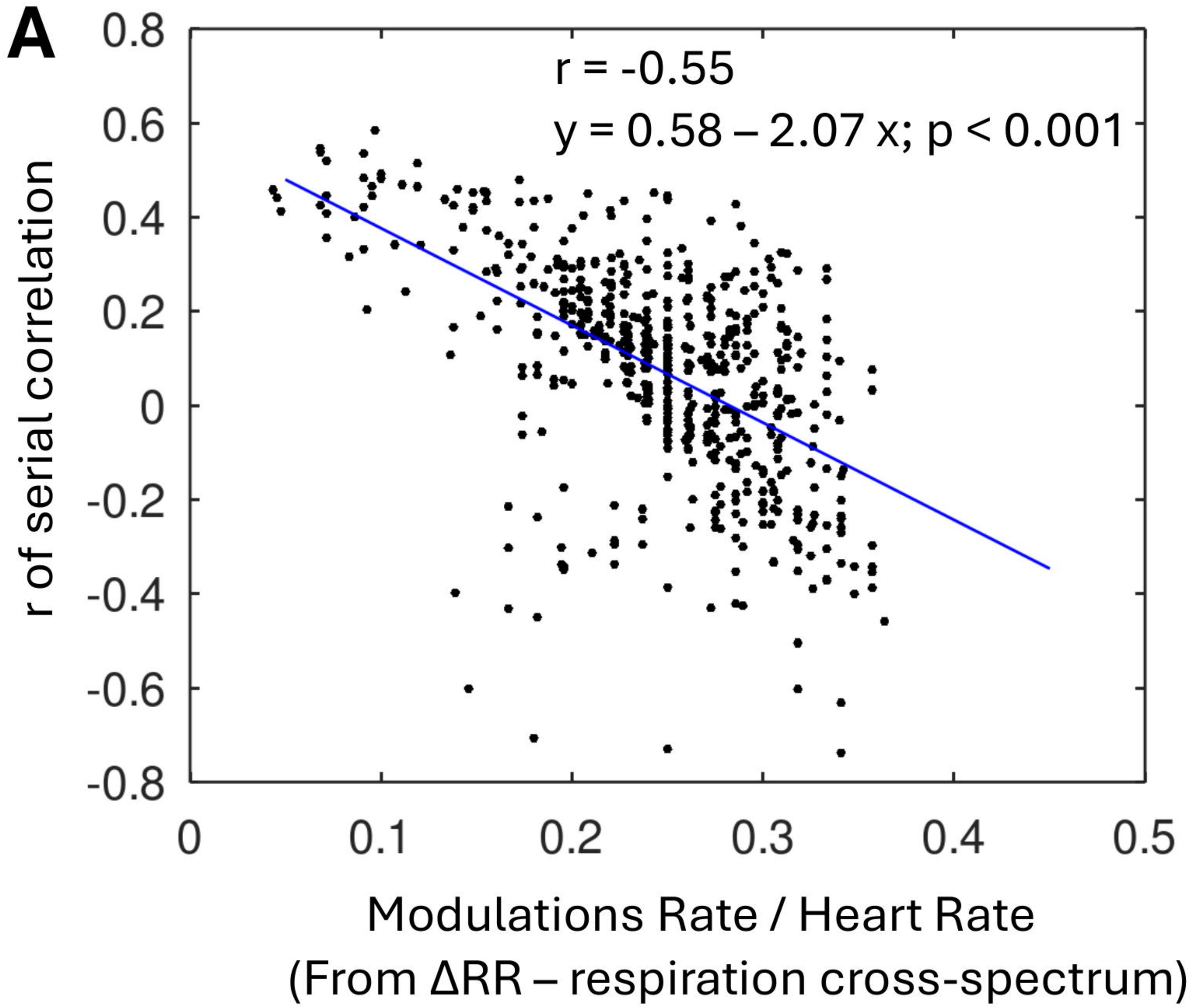
A
r = -0.55
y = 0.58 – 2.07 x; p < 0.001
r of serial correlation
0.8
0.6
0.4
0.2
0
-0.2
-0.4
-0.6
-0.8
0
0.1
0.2
0.3
0.4
0.5
Modulations Rate / Heart Rate
(From ΔRR – respiration cross-spectrum)

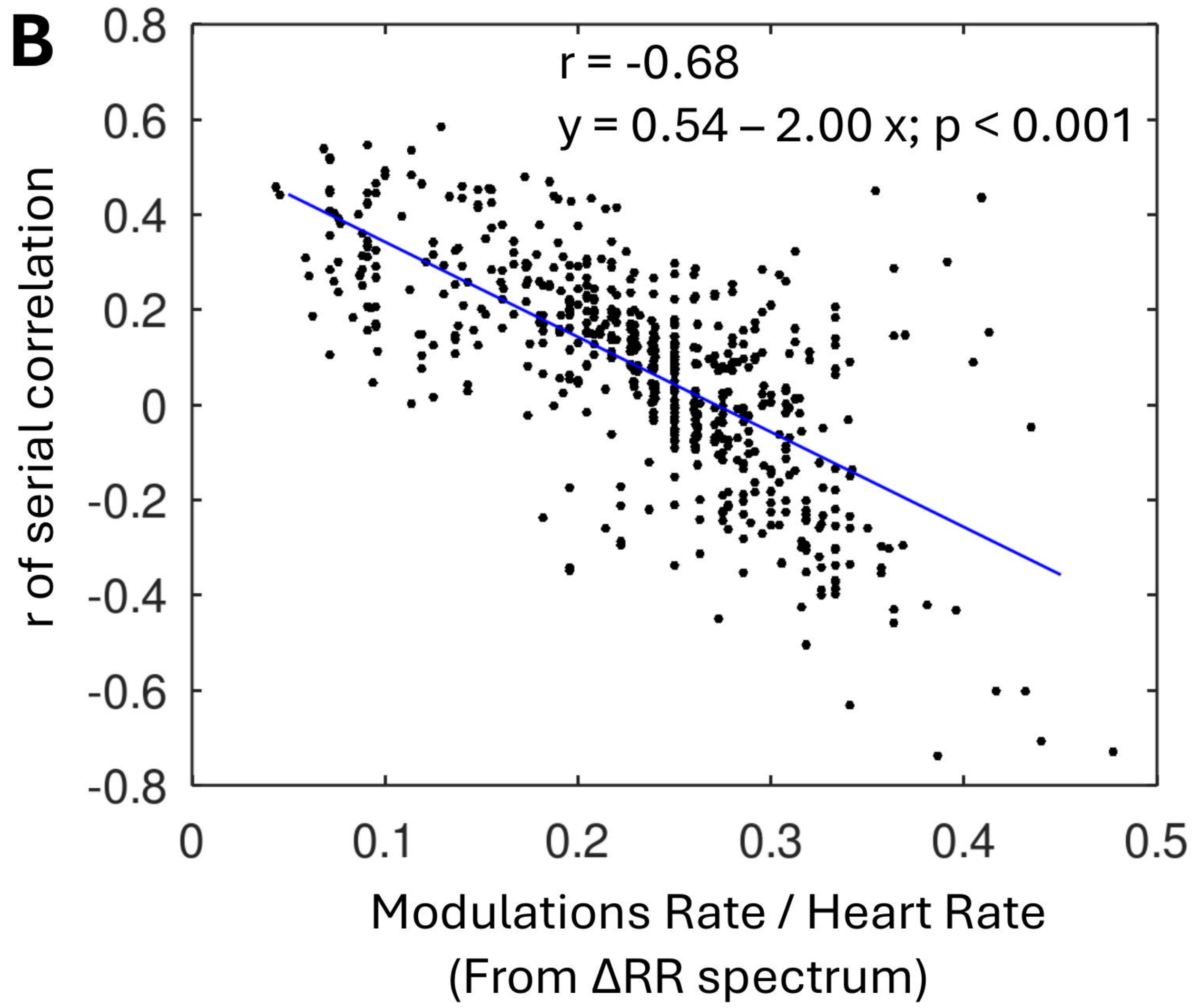
B
r = -0.68
y = 0.54 – 2.00 x; p < 0.001
r of serial correlation
0.8
0.6
0.4
0.2
0
-0.2
-0.4
-0.6
-0.8
0
0.1
0.2
0.3
0.4
0.5
Modulations Rate / Heart Rate
(From ΔRR spectrum)

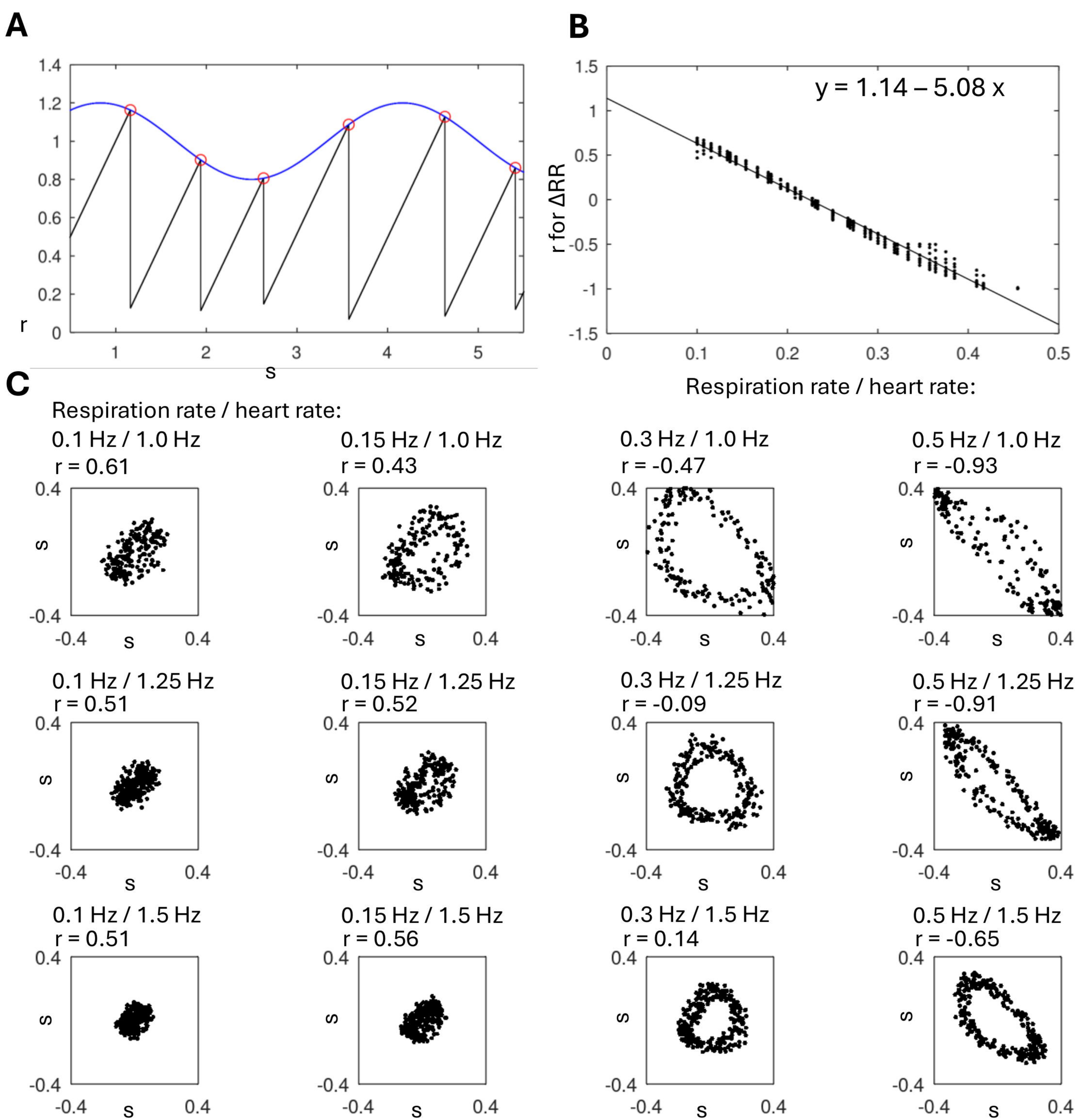
A
r
s
B
y = 1.14 – 5.08 x
r for ΔRR
C
Respiration rate / heart rate:
0.1 Hz / 1.0 Hz
r = 0.61
0.15 Hz / 1.0 Hz
r = 0.43
0.3 Hz / 1.0 Hz
r = -0.47
0.5 Hz / 1.0 Hz
r = -0.93
0.1 Hz / 1.25 Hz
r = 0.51
0.15 Hz / 1.25 Hz
r = 0.52
0.3 Hz / 1.25 Hz
r = -0.09
0.5 Hz / 1.25 Hz
r = -0.91
0.1 Hz / 1.5 Hz
r = 0.51
0.15 Hz / 1.5 Hz
r = 0.56
0.3 Hz / 1.5 Hz
r = 0.14
0.5 Hz / 1.5 Hz
r = -0.65